

Anodic Synthesis of Highly Ordered TiO₂ Nanotube Arrays: Role of Electrolyte Composition on the Structural, Morphological, Optical, and Photoelectrochemical Properties

Hawraa Sabah Hreo¹, Araa Mebdir Holi^{1,*}, and Asla Abdullah Al-Zahrani²

¹ Department of Physics, College of Education, University of Al-Qadisiyah, Al-Diwaniyah, Al-Qadisiyah 58002, Iraq

² Imam Abdulrahman Bin Faisal University, Eastern Region, Dammam, Saudi Arabia

Received 11 April 2022, Revised 16 July 2022, Accepted 17 August 2022

ABSTRACT

The fluoride species present in two different anodizing electrolytes were used to produce TiO₂ nanotube arrays (TiO₂ NTAs) by simultaneous anodic reaction and chemical dissolution. In this investigation, two different electrolytes were used for the preparation; [Eth. TiO₂ NAs: 95 ml ethylene glycol+0.5% NH₄F+5 ml DI water] and [Gly. TiO₂ NAs: 75 ml glycerine+0.5% NH₄F+25 ml DI water]. The effects of the prepared electrolytes used in the synthesis of TiO₂ nanotube arrays on structural element composition, morphology, and optical properties are the focus of this study and are characterized by X-ray diffraction (XRD), scanning electron microscopy field emission (FE-SEM), energy-dispersive X-ray spectroscopy (EDX) and UV-vis diffusion reflection spectroscopy (DRS), respectively. The photoelectrochemical properties of TiO₂ NTAs prepared in different electrolytes were investigated. The photoelectrochemical performance of TiO₂ NTAs in Na₂SO₃ (0.1 M) and Na₂S (0.1) was examined under the light of 100 mW/cm² from a xenon lamp. When we compare the photoelectrochemical (PEC) results of both electrolytes, we find that Eth. TiO₂ NTAs contribute a wide surface area resulting in an enhanced PEC response. TiO₂ NTs, which were prepared with Eth. TiO₂ NTAs, exhibited the highest photocurrent density, 0.326 mA cm⁻², and photoconversion efficiency (0.22%).

Keywords: Anodizing method, Electrolyte composition, Glycerine and ethylene glycol TiO₂ nanotube arrays

1. INTRODUCTION

TiO₂ NTAs is a well-known material that is widely used in a variety of applications, including photoelectrochemical cells [1-2]. Because of its high resistance, photoelectrochemical performance, nontoxicity, and low cost, TiO₂ NTAs is widely regarded as a top semiconductor material for photoanodes in photoelectrochemical applications [3]. There have been numerous attempts to produce titanium dioxide nanotubes over the years, such as vapor deposition [4], the sol-gel method [5-6], and there is also the hydrothermal process [7-8]. Toxic chemicals, long times, and even high temperatures are some of the drawbacks of these processes. TiO₂ NTAs can be produced using a simple anodization process, which only requires nontoxic materials and can be done at room temperature [9-11]. The bandgap of TiO₂ NTAs is only 3.2 electron volts. Because such nanostructured metal oxides can be employed in a variety of applications [12-13], including nanosized research and practical devices, the production of controlled nanoscale TiO₂ structures has gotten a lot of attention. Nanoparticles (NPs) are the most common nanostructure for TiO₂ applications, as they provide the key benefit of surface extension in a dense region. Nanorods (NRs) and nanotubes (NTs) are two other nanoscale TiO₂ structures of interest. TiO₂ nanotubes (TNTs) are a popular choice among them. TNTs that are well-ordered and tightly packed have various advantages.

Note: Accepted manuscripts are articles that have been peer-reviewed and accepted for publication by the Editorial Board. These articles have not yet been copyedited and/or formatted in the journal house style.

Potentiostatic anodization is currently the simplest approach for producing highly ordered TNTs with precise thickness control as well as length [14-15]. When it comes to the TiO₂ NTs, the growth conditions determine their chemical and physical properties [16]. Thus, by adjusting growth parameters such as anodization time, electrolyte composition, and an applied voltage, the morphology of NTs can vary greatly [17].

In this paper, we focused on electrolyte composition and its effect on the length, diameter, and thickness of the wall of TNTs and discussed their photoelectrochemical performance.

2. MATERIAL AND METHODS

2.1 Preparation of TiO₂ Nanotube arrays

The first step was to cut a sheet of 99.9 percent pure titanium foil into (2.5x1) cm². Following that, the pieces were chemically reduced by using an ultrasonic treatment in acetone, isopropanol, or deionized water (DI water) for fifteen minutes. After that, they were immersed for 10 minutes in a solution of 6 M HNO₃ to smooth out the surface [18]. Using a high-density two-electrode cell, the anodizing of titanium foil was accomplished. High-density graphite served as the opposing electrode, and the titanium foil served as the working electrode. The distance between two electrodes was maintained at two centimeters throughout the experiment. A DC power supply (MP6010D) was used to anodize the Ti after one hour of anodization at 40V, as shown in Figure 1. An electrolytic composition was then used to do the anodization process. The following is a list of TiO₂ nanotubes (TNT) preparation: Step 1; [95 ml ethylene glycol + 5 ml DI water + 0.5% NH₄F] and Step 2; [75 ml glycerine + 25 ml DI water + 0.5% NH₄F], which were both samples labelled Eth. TiO₂ NTAs and Gly. TiO₂ NTAs, respectively. The samples were rinsed with DI water after they had been prepared. In a thermo-oven, the films were annealed for 2 hours at 500 degrees Celsius.

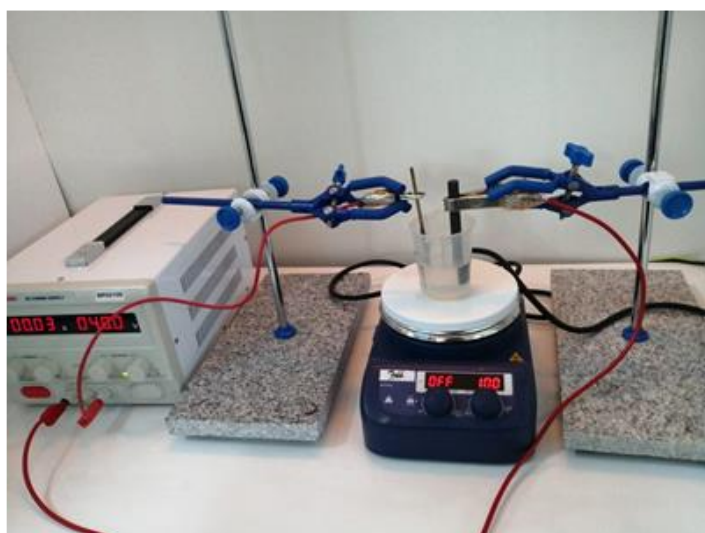


Figure 1. Setup for anodization method.

2.1.1 Characterization of TiO₂ Nanotube arrays

In order to determine the photoanodes' XRD patterns, we used the Shimadzu LabX XRD-6000 X-ray Diffractometer with a scanning range of 10°– 80° (2θ). The morphologies of the photoanodes were investigated using a field emission scanning electron microscope (Nova Nano

SEM 450) in conjunction with energy-dispersive X-ray spectroscopy (EDS). The Shimadzu TM model DUV 3700 Spectrophotometer was used to perform UV-Vis diffuse reflectance spectroscopy (DRS) in the wavelength range of (200 - 800) nm. To evaluate the photoelectrochemical performance of TiO₂ nanotubes, a three-electrode electrochemical cell was constructed in order to conduct photoelectrochemical measurements. The three electrodes used were TiO₂ NTAs samples as working electrodes, platinum (Pt) wire as a counter electrode, and silver/silver chloride (Ag/AgCl) as references electrode. The electrolyte cell was created by mixing Na₂SO₃ (0.1 M) with Na₂S (0.1 M). The linear sweep voltammetry (LSV) technique measured photocurrent density using TiO₂ nanotubes (Gamry Instrument framework interface with 1000 E Potentiostat/Galvanostat/ZRA). By utilising Fully Reflective Solar Simulator (SS1.6kW) the effect of the potential between (-1.2 and +1.2 V) versus Ag/AgCl at a scan rate of 20 mVs⁻¹ was found. Newport's xenon lamp simulated solar irradiation in the atmosphere and on the ground. By ASTM G173-03(2012), the lamp's output intensity was matched to the spectrum of solar irradiance. The xenon lamp's light was focused on a quartz reaction cell (15 cm apart) with a working electrode area of 1 cm. The manual chopping was used as the light source at regular intervals and had an irradiance of 100 mW/cm², equivalent to one sun lighting. The photoconversion efficiency (η) of the proposed TiO₂ NTAs was evaluated using the expression [19]:

$$\eta = \frac{J_{ph} (1.23 - V_{app})}{P_{in}} \times 100\% \quad (1)$$

where J_{ph} is the photocurrent density in (mA/cm²), V_{app} is the applied voltage in (V), the standard reversible redox potential of water electrolysis [vs. the normal hydrogen electrode (NHE)] is denoted as 1.23 V, and P_{in} is the power intensity of the illumination in (mW/cm²).

3. RESULTS AND DISCUSSION

3.1 Structural analysis

Figure 2 shows the XRD patterns of Ti, Eth.TiO₂ NTAs, and Gly.TiO₂ NTAs from 10° to 80° (2-theta). The first pattern displays peaks of Ti diffraction that correspond to metallic Ti used as a substrate for the anodization procedure. After anodizing Ti foil, all of the new peaks have matched to the standard tetragonal TiO₂ anatase phase (JCPDS card number 021-1272) and TiO₂ rutile phase (JCPDS card 021-1276). Crystallinity is good enough to see the highest peak of Eth. TiO₂ NTs at 25.47° of an anatase phase in the lattice plane of (101). Numerous studies confirm this conclusion [20-21], and the highest peak of Gly. TiO₂ NTAs at 25.30° of an anatase phase in the lattice plane (101). Debye-formula Scherer's was used to determine the crystallite size (D) [22]. The crystallite sizes of Eth. TiO₂ NTAs and Gly. TiO₂ NTAs were 28.2nm and 32.8nm, respectively.

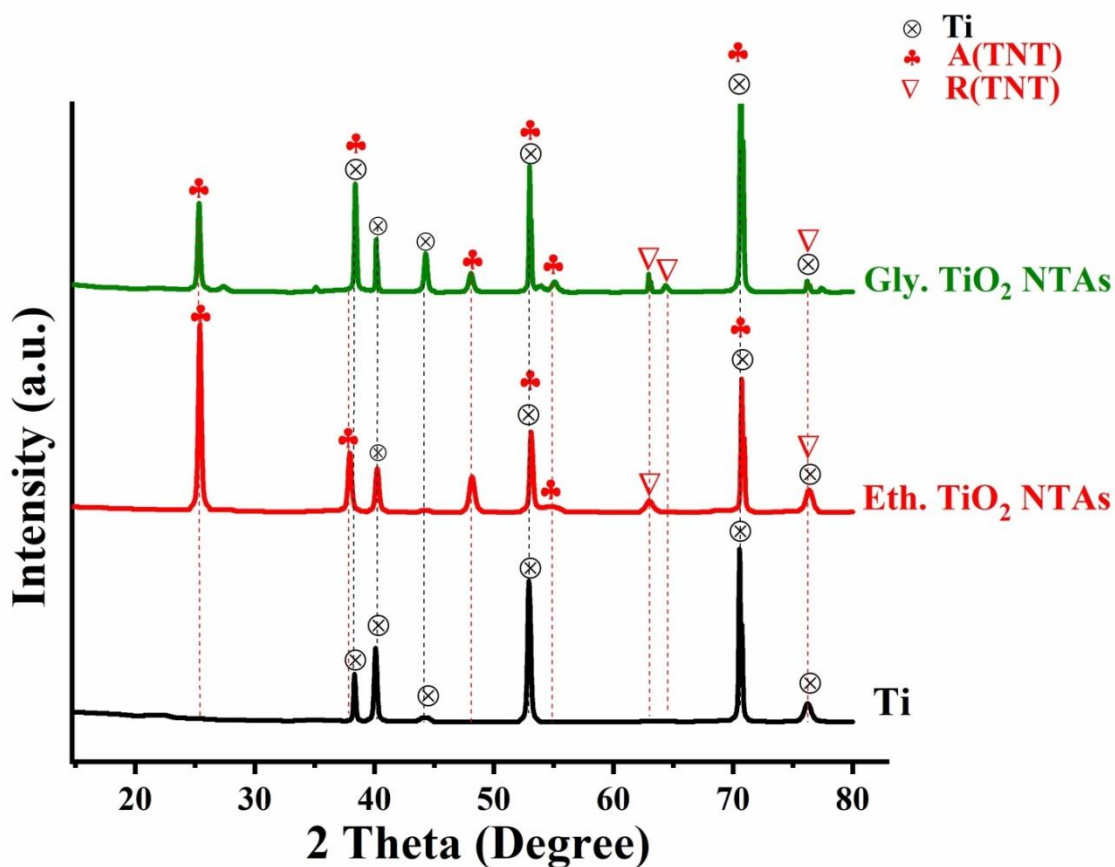


Figure 2. XRD patterns of Ti Foil, and TiO₂ NTAs prepared at various electrolyte compositions of A: (ethylene glycol + NH₄F + DI water); and B: (glycerin + NH₄F + DI water).

3.2 Morphological and EDS analysis

Figure 3 illustrates the morphology of Eth. TiO₂ NTAs and Gly. TiO₂ NTAs. Titanium foil was anodized in different electrolytes for 60 minutes. However, the self-ordered morphology of Eth. TiO₂ NTAs and Gly. TiO₂ NTAs were not the same on the surface which could clearly be seen in Figure 3. Digimizer image analysis software was used to determine the average diameter of TiO₂ NTAs, which came out to around 70±0.20 nm of Eth. TiO₂ NTAs and 100±0.25 nm of Gly. TiO₂ NTAs. The cross-sectional images of these samples are shown in Figure 4. As illustrated in Figure 4A, Eth. TiO₂ NTAs are smooth, aligned, and thin wall thickness with a length of roughly 7±0.600 μm. However, the morphological form of anodized titanium samples changed dramatically as the concentrations of electrolytes changed to (ethylene glycol + NH₄F + DI water). In comparison to Eth. TiO₂ NTAs, Gly. TiO₂ NTAs have a large diameter, thick wall thickness and a shorter length of around 5±0.300 μm. As the electrolyte viscosity increased, the nanotube growth in glycerine solution became shorter in length and larger in diameter, as illustrated in Figure 4B. As mentioned earlier, the synthesis and growth rate of TiO₂ nanotubes are adversely affected by viscosity [23]. Glycerin-based electrolytes had a low growth rate, but the addition of water increased the growth rate by lowering the viscosity of the electrolyte solution. Because it is less viscous than glycerol, ethylene glycol has lower diffusion resistance. As a result, the growth rate in ethylene glycol electrolytes was higher.

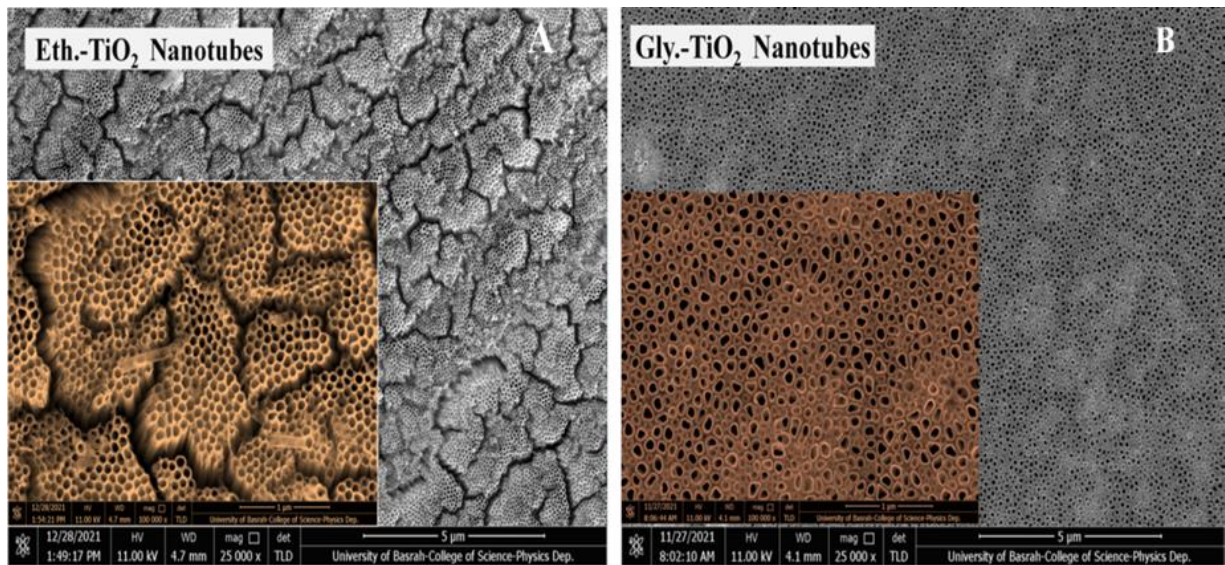


Figure 3. FESEM images of TiO_2 NTAs prepared at various electrolyte compositions of A: (ethylene glycol + NH_4F + DI water); and B: (glycerin + NH_4F + DI water).

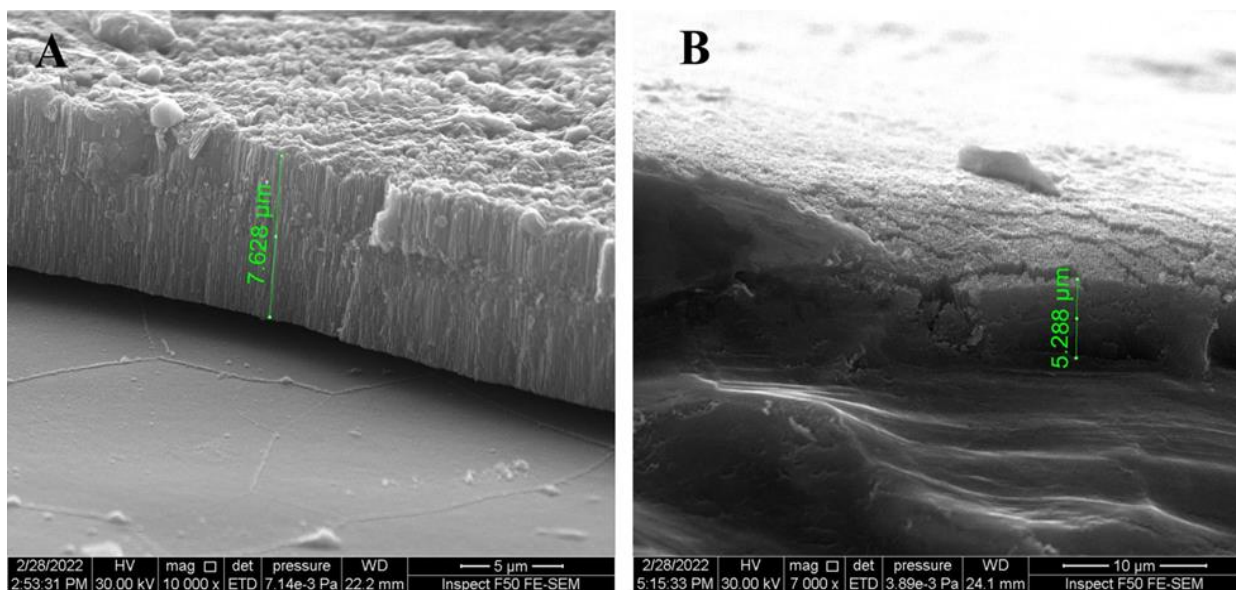


Figure 4. FESEM images of cross sectional of TiO_2 NTAs prepared at various electrolyte compositions of A: (ethylene glycol + NH_4F + DI water); and B: (glycerin + NH_4F + DI water).

In order to confirm TiO_2 formation, EDX was performed. During the EDX measurement areas were focused and the corresponding peaks are shown in Figure 5. As shown in the inset of Figure 5, the quantity of C, O, and Ti were measured in atomic %. The EDX results detected carbon (C), which is due to the high background counts in EDX, which results in an artificial carbon (C) peak [24]. As a result, even if the sample does not contain carbon, it is routinely measured. The results of elemental mapping for the TiO_2 nanostructures (shown in Figure 6) distinctly illustrate the existence of Ti, O, and C elements in the Eth. TiO_2 NTAs and Gly. TiO_2 NTAs samples, respectively.

Note: Accepted manuscripts are articles that have been peer-reviewed and accepted for publication by the Editorial Board. These articles have not yet been copyedited and/or formatted in the journal house style.

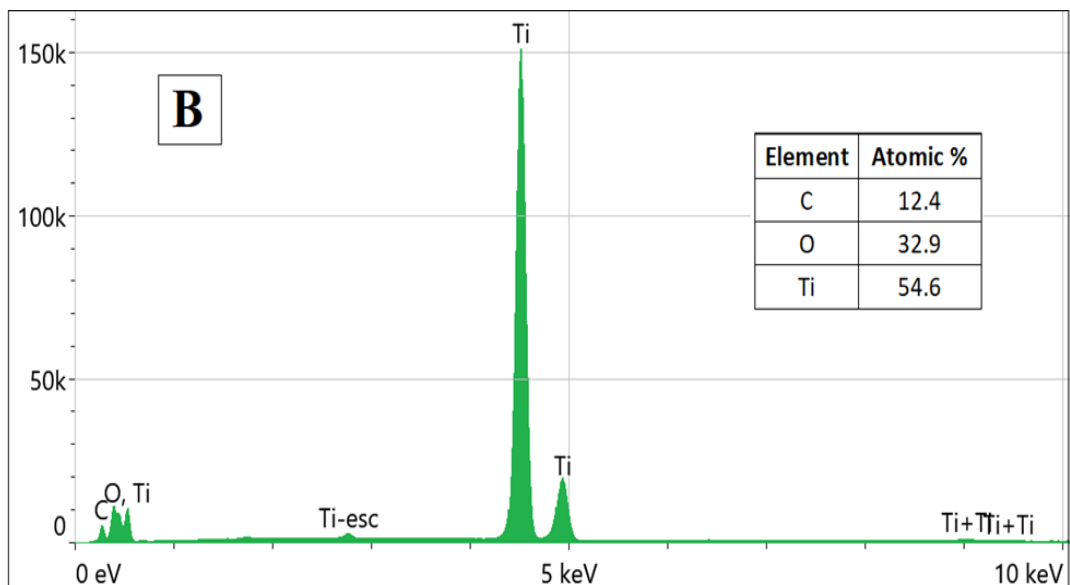
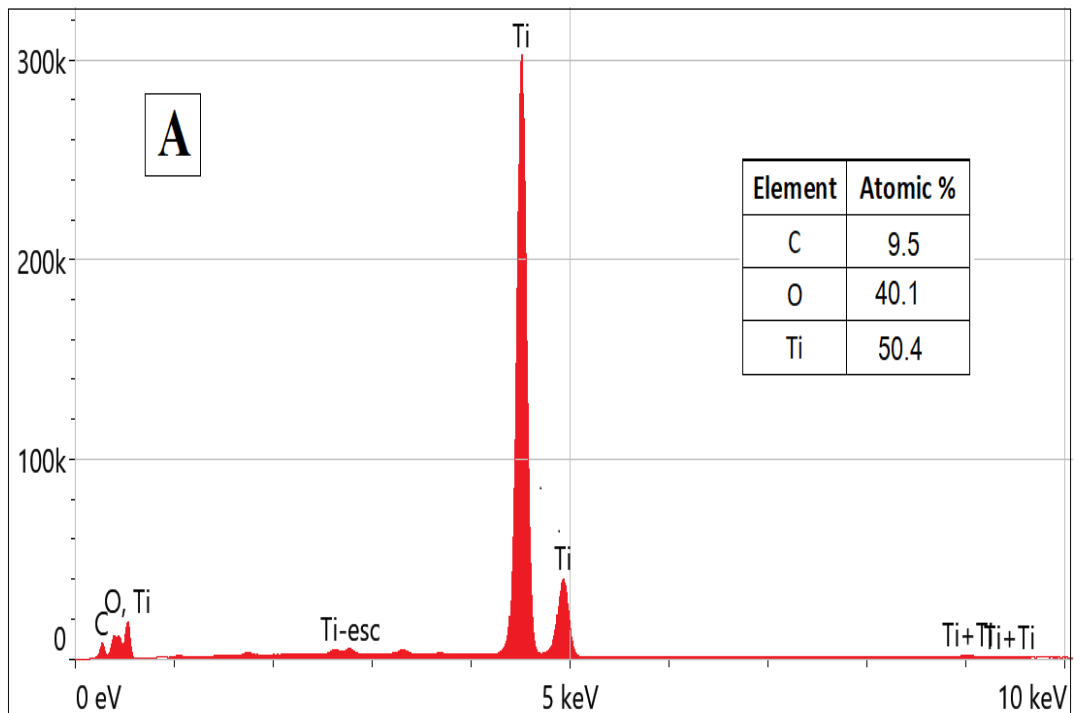


Figure 5. EDX spectra of TiO_2 NTAs prepared using different electrolyte compositions of A: (ethylene glycol + NH_4F + DI water); and B: (glycerin + NH_4F + DI water).

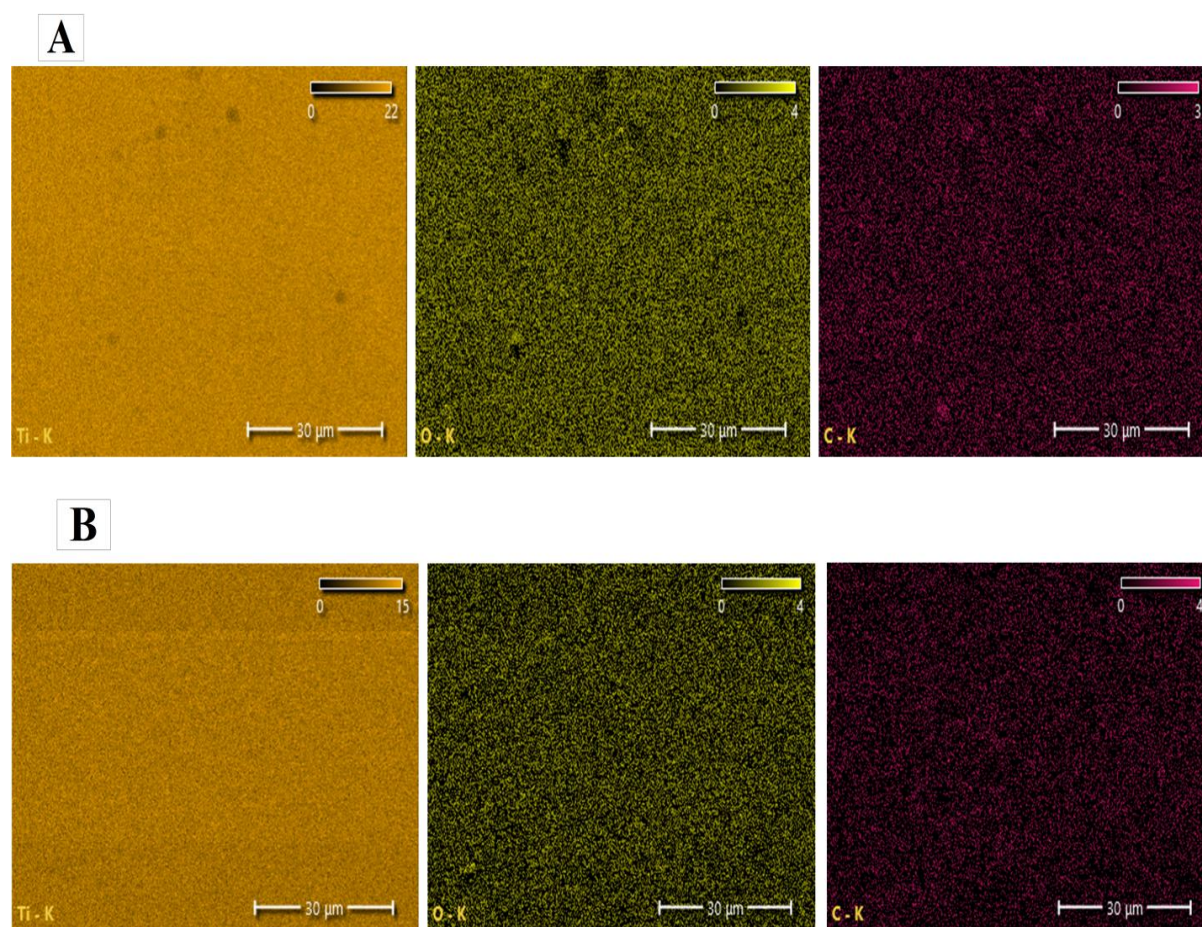


Figure 6. Elemental mapping of TiO₂ nanotubes prepared using different electrolyte compositions of A: (ethylene glycol + NH₄F + DI water); and B: (glycerin + NH₄F + DI water).

3.3 Optical properties

Figure 7 shows UV-vis diffuse reflectance spectra (DRS) of Eth. TiO₂ NTAs and Gly. TiO₂ NTAs produced with various electrolyte compositions. According to spectral data, TiO₂ NTAs absorb the most UV light below 400 nm. Table 1 shows the TiO₂'s absorption edges and energy gaps values.

Table 1 Absorption edges and Energy gap values of TiO₂ NTAs with different electrolytes

Photoanode construction	Absorption edges (nm)	Eg (eV)
Eth.TiO ₂ NTAs	387	3.2
Gly.TiO ₂ NTAs	375	3.3

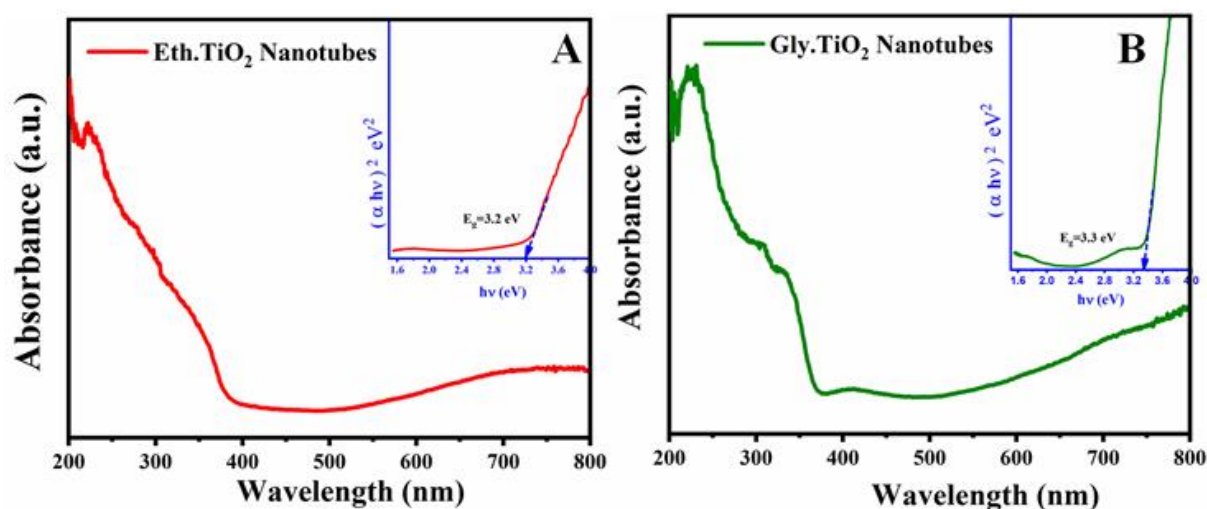


Figure 7. Elemental mapping of TiO₂ nanotubes prepared using different electrolytes compositions of A: (ethylene glycol + NH₄F + DI water); and B: (glycerin + NH₄F + DI water).

3.4 PEC performance

Figure 8 depicts the photocurrent response of Eth. TiO₂ NTAs and Gly. TiO₂ NTAs fabricated in diverse electrolytes. Comparing the two types of TiO₂ NTAs in terms of their photoresponse due to the longer tube, TiO₂ NTAs in ethylene glycol exhibit a higher photocurrent response (0.326 mA/cm²) than TiO₂ NTAs in glycerine (0.196 mA/cm²). This conclusion is consistent with the researcher's findings [25]. The higher photocurrent density was explained by the larger active surface area of the photoanode, which improves light-gathering and photon absorption. The following empirical equations can calculate the valence and conduction bands of Eth. TiO₂ NTAs and Gly. TiO₂ NTAs [26-27].

$$E_{C.B.} = \chi - 0.5 E_g + E_o \quad (2)$$

$$E_{V.B.} = E_{C.B.} + E_g \quad (3)$$

Here $E_{V.B.}$ and $E_{C.B.}$ are the valence and conduction band edge potentials. The value of χ denotes the electronegativity of the constituent atoms, whereas E_o is the scaling factor describing the redox level of the reference electrode to the vacuum ($E_o = -4.5$ eV) and E_g denotes the semiconductor's bandgap energy. Table 2 shows the results of the above equations, with the χ value of TiO₂ being 5.82 eV [28]. At 0.5 V applied voltage, the photoconversion efficiency (η) of Eth. TiO₂ NTAs and Gly. TiO₂ NTAs photoelectrodes was 0.22% and 0.14%, respectively. The crucial aspect is that as the tubes get shorter, the surface area to volume ratio decreases. This explains why Gly. TiO₂ NTAs have a low collection efficiency. Long and highly ordered nanotubes, as shown by FESEM image Figure 4A, are desirable because they induce the photocurrent intensity to increase as tube length increases.

Table 2 The Values of C.B and V.B for TiO₂ NTAs prepared at various electrolyte compositions of A: (ethylene glycol + NH₄F + DI water); and B: (glycerine + NH₄F + DI water).

Photoanode construction	E_g (eV)	vs. NHE		vs. Vacuum	
		C.B (eV)	V.B (eV)	C.B (eV)	V.B (eV)
Eth. TiO ₂ NTAs	3.2	-0.300	2.900	-4.200	-7.400

Gly. TiO ₂ NTAs	3.3	-0.330	2.970	-4.175	-7.475
----------------------------	-----	--------	-------	--------	--------

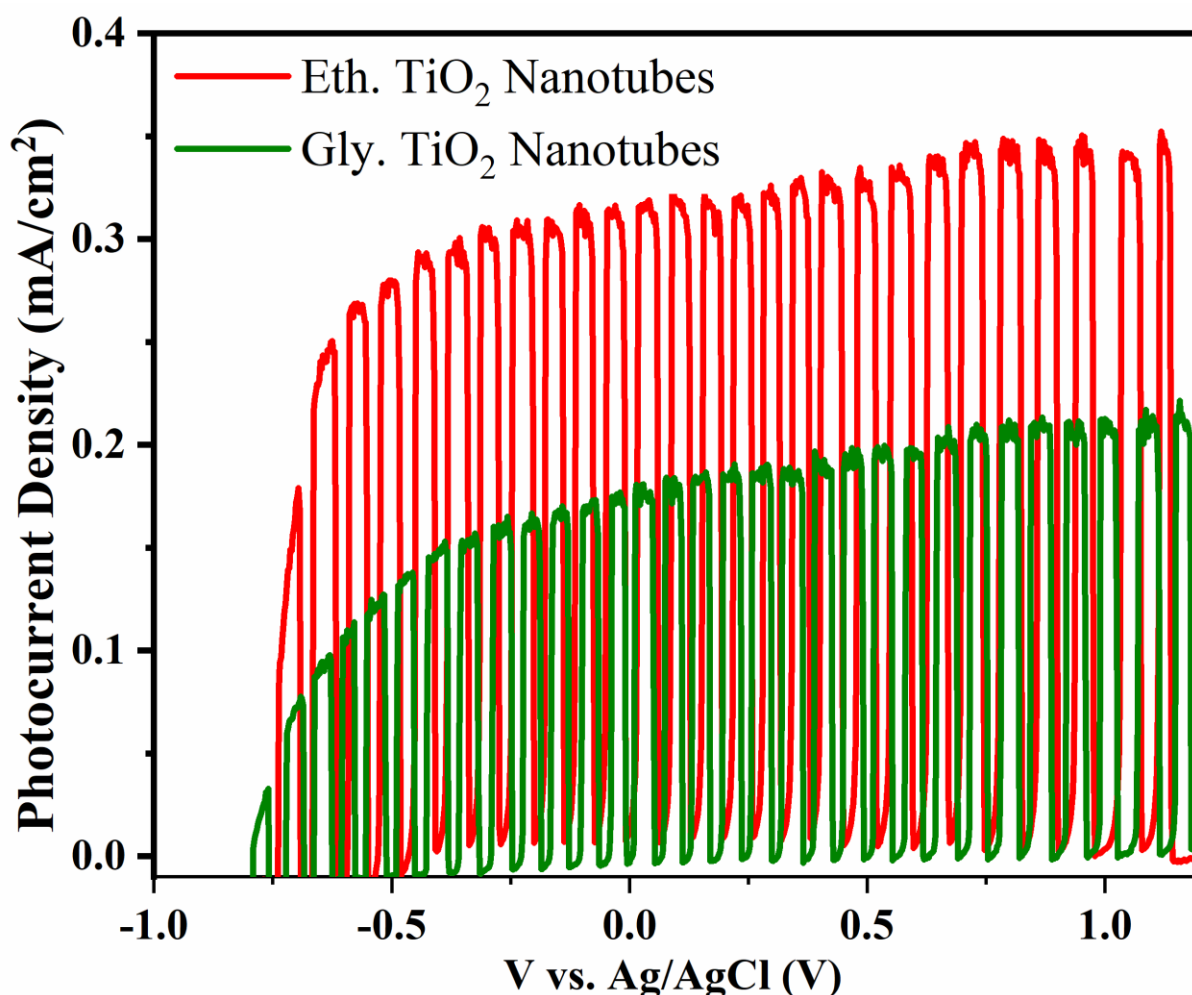


Figure 8. Linear sweep voltammograms obtained at the scan rate of 20 mV s^{-1} at applied potentials from -1.0 V to $+1.0 \text{ V}$ under illumination intensity of 100 mWcm^{-2} for plain TiO₂ NTAs prepared by different electrolytes.

4. CONCLUSION

An effective method has been studied to fabricate titanium dioxide nanotube arrays (TiO₂ NTAs) with two different solution compositions of ethylene glycol and glycerine. According to the results obtained using ethylene glycol, the highest photoresponse which is more efficient photoconversion compared to glycerine was obtained. In summary, the electrolyte plays an important role in influencing the crystal structure, morphology, and PEC performance.

ACKNOWLEDGEMENTS

We would like to show our appreciation to the Department of Physics, College of Education, University of Al-Qadisiyah, Iraq, for the experimental support of this research work and special thanks to Imam Abdulrahman Bin Faisal University, Saudi Arabia.

Note: Accepted manuscripts are articles that have been peer-reviewed and accepted for publication by the Editorial Board. These articles have not yet been copyedited and/or formatted in the journal house style.

REFERENCES

- [1] Ito, S., Chen, P., Comte, P., Nazeeruddin, M. K., Liska, P., Péchy, P., & Grätzel, M. Fabrication of screen-printing pastes from TiO₂ powders for dye-sensitized solar cells. *Progress in photovoltaics: research and applications*, 15(2007) 603-612.
- [2] Linsebigler, A. L., Lu, G., & Yates Jr, J. T. Photocatalysis on TiO₂ surfaces: principles, mechanisms, and selected results. *Chemical reviews*, 95(1995) 735-758.
- [3] Marques, J. O., Bellato, C. R., de Souza, C. H., Silva, R. C. D., & Rocha, P. A. Synthesis, characterization and enhanced photocatalytic activity of iron oxide/carbon nanotube/Ag-doped TiO₂ nanocomposites. *Journal of the Brazilian Chemical Society*, 28(2017) 2301-2312.
- [4] Kim, Y. S., Song, M. Y., Park, E. S., Chin, S., Bae, G. N., & Jurng, J. Visible-light-induced bactericidal activity of vanadium-pentoxide (V₂O₅)-loaded TiO₂ nanoparticles. *Applied biochemistry and biotechnology*, 168(2012) 1143-1152.
- [5] Tsvetkov, N., Larina, L., Ku Kang, J., & Shevaleevskiy, O. Sol-gel processed TiO₂ nanotube photoelectrodes for dye-sensitized solar cells with enhanced photovoltaic performance. *Nanomaterials*, 10(220) 296.
- [6] Huang, C., Liu, X., Liu, Y., & Wang, Y. Room temperature ferromagnetism of Co-doped TiO₂ nanotube arrays prepared by sol-gel template synthesis. *Chemical physics letters*, 432(2006) 468-472.
- [7] Zavala, M. Á. L., Morales, S. A. L., & Ávila-Santos, M. Synthesis of stable TiO₂ nanotubes: effect of hydrothermal treatment, acid washing and annealing temperature. *Heliyon*, 3(2017) e00456.
- [8] Perera, S. D., Mariano, R. G., Vu, K., Nour, N., Seitz, O., Chabal, Y., & Balkus Jr, K. J. Hydrothermal synthesis of graphene-TiO₂ nanotube composites with enhanced photocatalytic activity. *Acs Catalysis*, 2(2012) 949-956.
- [9] Pishkar, N., Ghoranneviss, M., Ghorannevis, Z., & Akbari, H. Study of the highly ordered TiO₂ nanotubes physical properties prepared with two-step anodization. *Results in Physics*, 9(2018) 1246-1249.
- [10] Sopha, H., Norikawa, Y., Motola, M., Hromadko, L., Rodriguez-Pereira, J., Cerny, J., ... & Macak, J. M. Anodization of electrodeposited titanium films towards TiO₂ nanotube layers. *Electrochemistry Communications*, 118(2020) 106788.
- [11] Ghani, T., Mujahid, M., Mehmood, M., Ubaidullah, M., Shah, A., & Mahmood, A. Effect of Processing Temperature on the Morphology and Crystal Structure of Anodic TiO₂ Nanotubes. *Journal of Electronic Materials*, 49(2020) 1881-1888.
- [12] Holi, A. M., and AL-Zahrani, A. A. Spin Coating Technique for the Synthesis of Hexagonal Cd_xZn_{1-x}S Decorated Pure ZnO Nanorods Arrays. *Int. J. Nanoelectron. Mater.* 13 (2020) 121-129.
- [13] AL-Zahrani, A. A., Zainal, Z., Talib, Z. A., Ngee, J. L. H., Mohd, L., Fudzi, A. M. H., & Ali, M. Effect of Hydrothermal Growth Temperature and Time on Physical Properties on Photoanode Performance of ZnO Nanorods. *Int. J. Nanoelectron. Mater.*, 13(2020)381-400.
- [14] Momeni, M. M., & Mozafari, A. A. The effect of a number of SILAR cycles on morphological, optical, and photo catalytic properties of cadmium sulfide-titania films. *Journal of Materials Science: Materials in Electronics*, 27((2016) 10658-10666.
- [15] Dagherir, R., Drogui, P., & Robert, D. Modified TiO₂ for environmental photocatalytic applications: a review. *Industrial & Engineering Chemistry Research*, 52(2013) 3581-3599.

- [16] Li, D. G., Chen, D. R., Wang, J. D., & Liang, P. Effect of acid solution, fluoride ions, anodic potential and time on the microstructure and electronic properties of self-ordered TiO₂ nanotube arrays. *Electrochimica Acta*, 207(2017) 152-163.
- [17] Lai, Y., Lin, L., Pan, F., Huang, J., Song, R., Huang, Y., & Chi, L. Bioinspired patterning with extreme wettability contrast on TiO₂ nanotube array surface: a versatile platform for biomedical applications. *Small*, 9(2013) 2945-2953.
- [18] Ayal, A. K., Zainal, Z., Lim, H. N., Talib, Z. A., Lim, Y. C., Chang, S. K., & Holi, A. M. Photocurrent enhancement of heat treated CdSe-sensitized titania nanotube photoelectrode. *Optical and Quantum Electronics*, 49(2017) 1-11.
- [19] Dong, X., Huang, W., & Chen, P. In situ synthesis of reduced graphene oxide and gold nanocomposites for nanoelectronics and biosensing. *Nanoscale Res Lett*, 6(2011) 1-6.
- [20] FCai, F. G., Yang, F., Jia, Y. F., Ke, C., Cheng, C. H., & Zhao, Y. Bi₂S₃-modified TiO₂ nanotube arrays: easy fabrication of heterostructure and effective enhancement of photoelectrochemical property. *Journal of Materials Science*, 48(2013) 6001-6007.
- [21] Al-Sajad, G. A., Holi, A. M., AL-Zahrani, A. A., & Najm, A. S. Titania Nanotubes Arrays Based-Gas Sensor: NO₂-Oxidizing Gas and H₂-Reducing Gas. *Nano Biomedicine & Engineering*, 12(2020).
- [22] Louër, D., & Audebrand, N. Profile fitting and diffraction line broadening analysis. *Advances in x-ray analysis*, 41(1999) 556-565.
- [23] Mohamed, A.E.R., Kasemphaibulsuk N., Rohani, S. & Barghi, S. Fabrication of titania nanotube arrays in viscous electrolytes. *Journal of nanoscience and nanotechnology*, 10(2010), 1998-2008.
- [24] Liao, Yougui. Practical electron microscopy and database. An Online Book (2006).
- [25] Lim, Y. C., Zainal, Z., Tan, W. T., & Hussein, M. Z. Anodization parameters influencing the growth of titania nanotubes and their photoelectrochemical response. *International Journal of Photoenergy*, 2012.
- [26] Helal, A., Harraz, F. A., Ismail, A. A., Sami, T. M., & Ibrahim, I. A. Hydrothermal synthesis of novel heterostructured Fe₂O₃/Bi₂S₃ nanorods with enhanced photocatalytic activity under visible light. *Applied Catalysis B: Environmental*, 213(2017) 18-27.
- [27] Holi, A. M., Zainal, Z., Ayal, A. K., Chang, S. K., Lim, H. N., Talib, Z. A., & Yap, C. C. Effect of heat treatment on photoelectrochemical performance of hydrothermally synthesised Ag₂S/ZnO nanorods arrays. *Chemical Physics Letters*, 710(2018) 100-107.
- [28] Yu, J., Xiang, S., Ge, M., Zhang, Z., Huang, J., Tang, Y., & Lai, Y. Rational Construction of LaFeO₃ Perovskite Nanoparticle-Modified TiO₂ Nanotube Arrays for Visible-Light Driven Photocatalytic Activity. *Coatings*, 8(2018) 374.